



The identification of novel 5'-amino gemcitabine analogs as potent RRM1 inhibitors



Marc A. Labroli^{a,*}, Michael P. Dwyer^b, Ruichao Shen^c, Janeta Popovici-Muller^c, Qinglin Pu^c, Daniel Wyss^a, Mark McCoy^a, Dianah Barrett^a, Nicole Davis^d, Wolfgang Seghezzi^d, Frances Shanahan^d, Lorena Taricani^d, Maribel Beaumont^d, Maria-Christina Malinao^d, David Parry^d, Timothy J. Guzi^c

^a Merck Research Laboratories, 2000 Galloping Hill Road, Kenilworth, NJ 07033, USA

^b Merck Research Laboratories, PO Box 2000, Rahway, NJ 07065, USA

^c Merck Research Laboratories, 33 Avenue Louis Pasteur, BMB-3, Boston, MA 02115, USA

^d Merck Research Laboratories, 901 South California Avenue, Palo Alto, CA 94304, USA

ARTICLE INFO

Article history:

Received 17 October 2013

Revised 29 January 2014

Accepted 7 February 2014

Available online 15 February 2014

Keywords:

Ribonucleotide reductase

Gemcitabine

CHK1

Deoxyribonucleotides

Oncology

ABSTRACT

The ribonucleotide reductase (RNR) enzyme is a heteromer of RRM1 and RRM2 subunits. The active enzyme catalyzes de novo reduction of ribonucleotides to generate deoxyribonucleotides (dNTPs), which are required for DNA replication and DNA repair processes. Complexity in the generation of physiologically relevant, active RRM1/RRM2 heterodimers was perceived as limiting to the identification of selective RRM1 inhibitors by high-throughput screening of compound libraries and led us to seek alternative methods to identify lead series. In short, we found that gemcitabine, as its diphosphate metabolite, represents one of the few described active site inhibitors of RRM1. We herein describe the identification of novel 5'-amino gemcitabine analogs as potent RRM1 inhibitors through in-cell phenotypic screening.

© 2014 Elsevier Ltd. All rights reserved.

tert-

1. Introduction

Ribonucleotide reductase (RNR) catalyzes the reduction of ribonucleotides to deoxyribonucleotides, the essential precursors of DNA synthesis. RNR is the rate limiting enzyme during de novo synthesis of deoxyribonucleotides (dNTPs).¹ RNR enzyme plays a central role in the maintaining a balanced supply of dNTPs required for DNA synthesis and repair. Thus, RNR plays an important role in genetic fidelity and cell viability.^{2,3} Of note, failure to adequately control dNTP levels leads to cell death and genetic abnormalities.^{4,5}

The classical ribonucleotide reductase of the de novo pathway comprises of two subunits, RRM1 and RRM2.¹ The large subunit, RRM1, contains the catalytic site, the substrate-specificity site and the activity site.³ The RRM2 subunit contains an iron center-generated tyrosyl free radical that can be scavenged by hydroxyurea.⁶ An additional RRM2 subunit, p53R2 has been identified.⁷

p53R2 can substitute for RRM2 to form an active enzyme with RRM1.⁸

The key role of RNR in DNA synthesis and cell growth has made it an important target for anticancer therapy.^{9–11} Non-selective inhibitors of RNR activity such as hydroxyurea (HU), clofarabine (CAFdA), gemcitabine (GEM), Trimidox, and Didox have been investigated for the treatment of a wide variety of solid tumors and hematologic malignancies.¹² Many of these agents suppress dNTP levels and inhibit DNA replication.^{13–15} Thus, exposure to multiple mixed-function non-selective DNA antimetabolites can induce a coordinated series of intra-S events that leads to replication fork stalling likely to participate in S-phase checkpoint activation.^{16,17}

2'-Deoxy-2',2'-difluorocytidine (gemcitabine) is an antimetabolite nucleoside approved for the treatment of pancreatic, breast, and non-small cell lung cancers either as a single agent or in combination with other chemotherapeutic agents.¹⁸ Gemcitabine is a prodrug which is intracellularly phosphorylated to active diphosphate and triphosphate forms.¹⁹ Gemcitabine diphosphate inhibits ribonucleotide reductase through binding to the active site of RRM1 leading to depletion of the deoxynucleotide pool and halt of DNA synthesis.²⁰ Gemcitabine triphosphate competes with deoxycytidine triphosphate for incorporation into DNA resulting

* Corresponding author. Tel.: +1 908 740 3168.

E-mail address: marc.labroli@merck.com (M.A. Labroli).

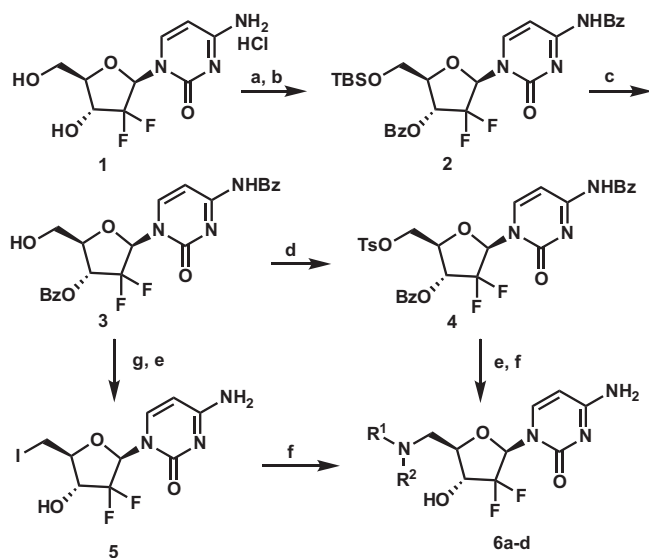
in termination of DNA polymerization.²¹ Together the effects elicited by individual gemcitabine metabolites result in the observed anticancer response.

Since the discovery of gemcitabine by Hertel et al.²² numerous gemcitabine derivatives have been synthesized in the search for new anticancer or antiviral agents.²³ For example, the base-modified gemcitabine derivatives include adenosine, guanine and uracil analogs.²⁴ The ribose-modified derivatives include 4'-azido analogs, 4'-allene substituted analogs, 3'-deoxy analogs, and thio/aza/carbocyclic analogs.^{25–28} However, due to the perceived requirement for phosphorylation of the 5'-OH to initiate the production of active NDP and NTP metabolites, replacement of the 5'-OH by other heteroatoms has been left virtually unexplored.

Crystal structures of RRM1 bound to the diphosphate metabolite revealed a discreet diphosphate binding pocket with phosphate binding mediated by a helix dipole interaction and several electrostatic interactions.²⁹ As our interest (vide supra) was in identification of selective RRM1 inhibitors, we hypothesized that gemcitabine diphosphate might serve as a template for the identification of such molecules. Thus, identification of 5'-substitution in replacement of the diphosphate with limited other structural changes may lead to effective competitors with the natural ligand. Likewise, the inability to form the triphosphate metabolite in situ would make these analogs devoid of competing incorporation into DNA. We focused our initial efforts on amine replacements for several reasons including the inability to revert back to gemcitabine (esp. in vivo) and ease of synthesis to rapidly test the hypothesis that something other than a diphosphate (or diphosphate mimic) would work.

2. Chemistry

The 5'-amino derivatives of gemcitabine, a class of synthetically accessible analogs capable of displaying diverse functionality that might catalyze binding to RRM1 have rarely been reported to date. We therefore embarked on an effort to prepare 5'-amino substituted gemcitabine analogs as novel RRM1 inhibitors. A variety of 5'-amino gemcitabine analogs were prepared according to the general scheme shown in Scheme 1 with several representative examples shown in Table 1.



Scheme 1. Reagents and conditions: (a) TBSCl, imidazole, DMF, rt, 12 h, 92%; (b) BzCl, DMAP, pyridine, rt, 12 h, 90%; (c) TBAF, THF, 0 °C, 3.5 h then AcOH, 85%; (d) TsCl, pyridine, Et₃N, 85%; (e) NH₃, MeOH, 92%; (f) R¹R²NH, DMF, 32–55%; (g) MeP(OPh)₃, DMF, 60 °C, 84%.

Table 1
Preparation of **6a–d** by S_N2 substitution

Entry	Amines	Product 6	Yield (%)
6a			32 ^a
6b			53 ^a
6c			53 ^b
6d			48 ^b

^a Heating at 100 °C.

^b Heating at 90 °C.

Our initial route to the 5'-amino-2',5'-dideoxy-2',2'-difluorocytidine analogs is outlined in Scheme 1. The synthesis began with protection of the 5'-hydroxy group of gemcitabine hydrochloride (**1**) as the butyldimethylsilyl (TBDMS) ether followed by global benzoyl protection to afford compound **2**. Desilylation of the 5'-TBDMS ether with tetrabutylammonium fluoride (TBAF) at 0 °C provided alcohol **3** followed by conversion to tosylate **4** under standard conditions. Treatment of intermediate **4** with 7 M NH₃ in MeOH cleaved the benzoate groups and the resulting tosylate was treated with the requisite amine with heating to afford products **6a,b** (Table 1). Alternatively, alcohol **3** was converted to the iodide intermediate **5** using methyltriphenoxyphosphonium iodide followed by benzoyl deprotection with 7 M NH₃ in MeOH. Treatment of iodide **5** with excess amine (3 equiv) at 90 °C provided 5'-amino-2',5'-dideoxy-2',2'-difluorocytidine analogs **6c,d** (Table 1). Utilization of iodide **5** allowed less amount of amine to be used in the final displacement reaction which made the purification of the final products more straightforward. The examples listed in Table 1 represent a limited set of compounds using the methodology outlined in Scheme 1 and further studies outlining the scope of this work has recently been published.³⁰

3. Biological results

3.1. H2AX assay

Complexity in the generation of physiologically relevant active RRM1/RRM2 complexes as a method for robust in vitro calibration of activity led us to seek alternative methods to characterize the novel compounds. Activation of the DNA replication checkpoint is one of the hallmarks of disruption of dNTP production by RNR. Previously, we had established a functional readout for override of the DNA replication checkpoint by monitoring gamma H2AX induction following treatment with the replication inhibitor hydroxyurea and CHK1 inhibitor SCH 900776.³¹ Similar induction of gamma H2AX was observed following knockdown of RRM1 with siRNA and subsequent treatment with SCH 900776 (unpublished

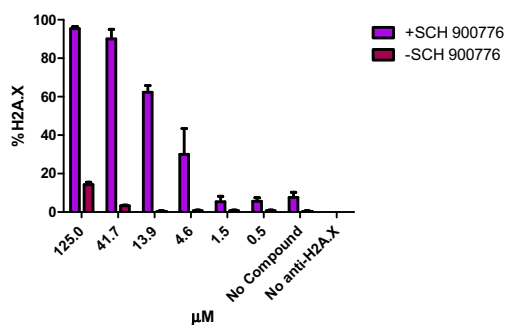
results). Hence, adaptation of this approach was reasoned to be effective in evaluating compounds for biological activity. Hence, treating cells with 5'-amino analogs **6a–d** overnight followed by exposure to SCH 900776 led to compound and dose dependent induction of H2AX (Fig. 1). These phenotypes matched those observed with the RRM1 siRNA knockdown (unpublished results) as well as that observed with gemcitabine shown in Figure 1. This assay was also useful for tracking SAR trends in a high throughput fashion. As depicted in Figure 1, compounds **6c,d** demonstrated a more pronounced response both in the presence and absence of SCH 900776 compared to **6a,b**. Moreover, comparison of **6d** to RRM1 inhibitor gemcitabine in this assay demonstrated comparable responses (Fig. 1). With in-cell demonstration of checkpoint activation in hand, it remained to prove that this series of compounds was acting in a mechanistically similar way to gemcitabine.

3.2. NMR binding studies

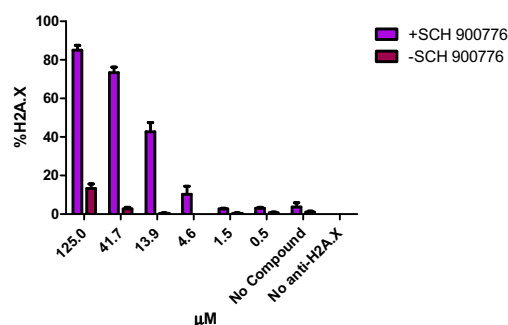
The large subunit of ribonucleotide reductase, RRM1, is a 90 kDa protein that binds nucleotides but has no enzymatic activity. In solution, RRM1 is a 180 kDa homodimer that is difficult to study structurally but is well-suited to ligand-detected NMR experiments. We probed ligand binding to RRM1 with 3 different NMR methods. Each method relies on different effects (line broadening, saturation transfer and NOE) that are transferred to the ligand and detected in its solution NMR spectrum.

Small molecule line broadening was detected in ^1H NMR spectra of **6d** acquired in the presence of RRM1 (Fig. 2). Ligand signals are reduced up to 27% by the addition of 1.8 μM RRM1 as compared to reference sample with the ligand and buffer but no protein. Signal reductions are a result of protein binding and are consistent with an approximate K_d of 200 μM .³² The DMSO peak

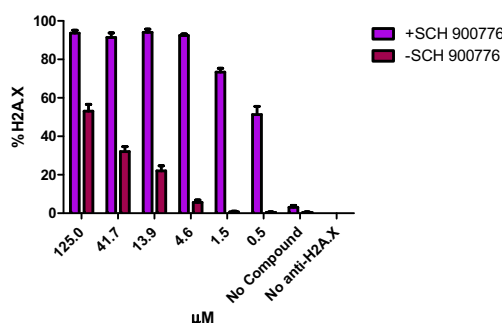
Anti-phospho H2A.X—U2OS cells Compound 6a o/n then exposed to +/- 0.5uM 900776



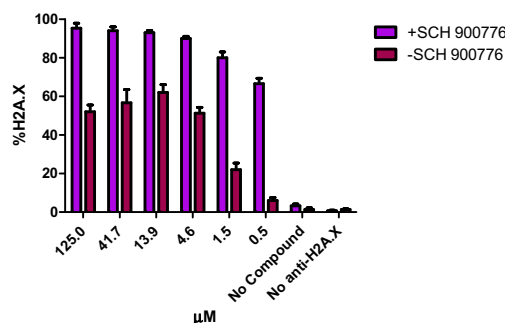
Anti-phospho H2A.X—U2OS cells Compound 6b o/n then exposed to +/- 0.5uM 900776



Anti-phospho H2A.X—U2OS cells Compound 6c o/n then exposed to +/- 0.5uM 900776



Anti-phospho H2A.X—U2OS cells Compound 6d o/n then exposed to +/- 0.5uM 900776



Anti-phospho H2A.X—U2OS cells gemcitabine o/n then exposed to +/- 0.5uM 900776

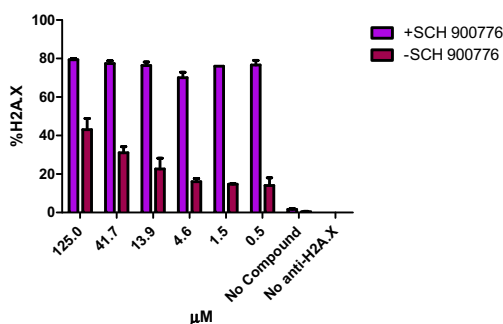


Figure 1. H2AX response for **6a–d** and gemcitabine in the presence and absence of SCH 900776.

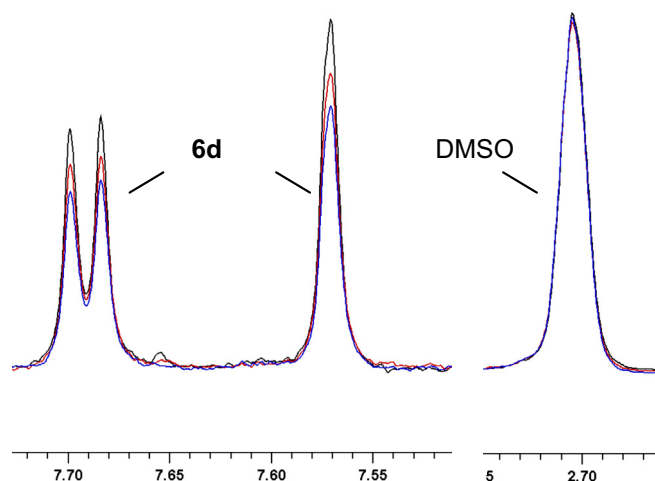


Figure 2. Compound binding to RRM1. Line-broadening in ^1H NMR spectra was used to assess **6d** binding to RRM1. The intensity of **6d** NMR peaks is reduced with increasing amounts of RRM1 protein (0, 0.9 and 1.8 μM), while the DMSO peak is unaffected. The decrease in peak intensity is due to line-broadening of **6d** while it is bound to RRM1.

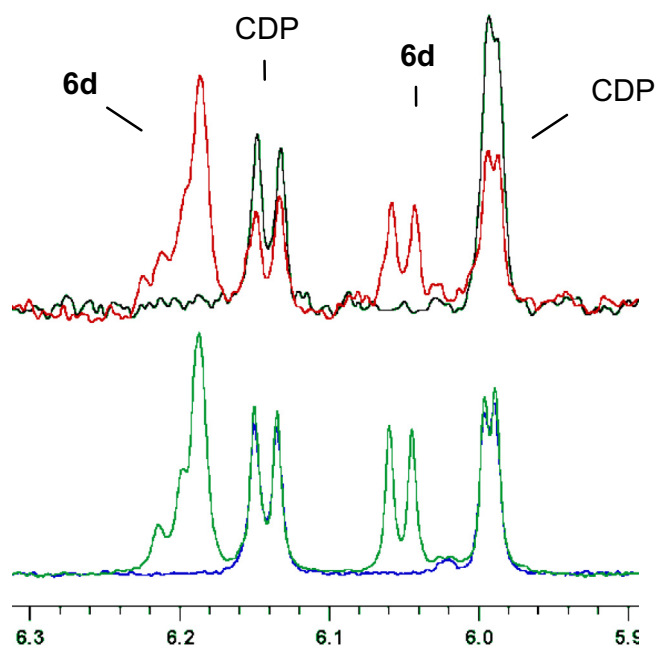


Figure 3. Binding of **6d** to the active site of RRM1. STD-NMR spectroscopy was used to test the ability of **6d** to compete with substrate. CDP binds to the active site of RRM1 and gives a large STD-NMR signal in the presence of 0.9 μM RRM1 (black). Addition of **6d** results in the appearance of new STD peaks for **6d** and a reduction of CDP STD-NMR peaks (red). ^1H NMR spectra for CDP (blue) and the CDP, **6d** mixture (green) are shown for reference.

was unaffected in these measurements and can be used as a reference. The binding of **6d** to RRM1 was also detected by saturation transfer difference NMR (STD-NMR).³³ Reference STD-NMR data was first acquired on CDP, which binds to the RRM1 active site and is a substrate of the active enzyme (Fig. 3). Addition of **6d** results in a new set of STD-NMR peaks for **6d**, from binding to RRM1, and a decrease of the CDP STD-NMR signal due to competition ($K_i \sim 150 \mu\text{M}$) with CDP.³⁴ Transferred NOESY experiments were carried out to obtain structural information on the RRM1-bound conformation of **6d**.³⁵ A single experiment with 9 μM RRM1

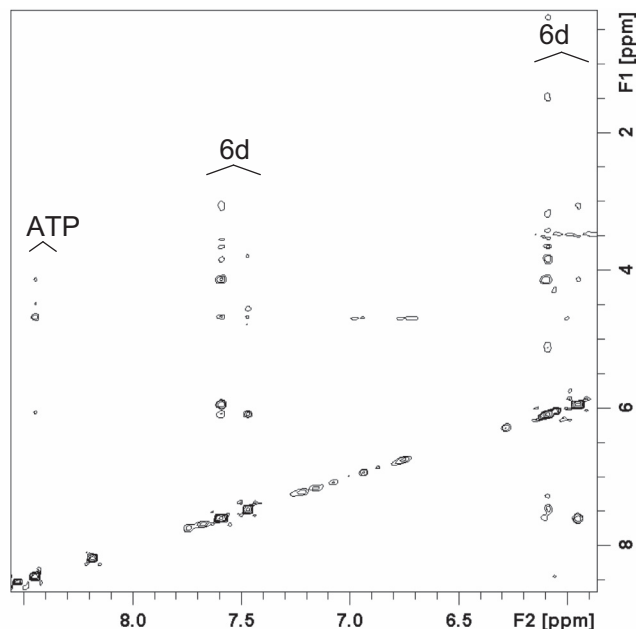


Figure 4. Structural data from transferred NOE experiments. A transferred NOE data set for a complex of RRM1, ATP and **6d** is shown. Both ATP and **6d** showed many NOE cross peaks that report on their RRM1-bound conformation.

yielded a number of ligand NOEs (Fig. 4) that are opposite in sign to NOEs of the free ligands. This data confirms RRM1 binding of both ATP and **6d** and provides ^1H - ^1H distance restraints on RRM1-bound **6d**.

3.3. NMR Activity Studies

^1H NMR measurements can also be used as a convenient read-out of RNR activity. RNR reactions require active enzyme, ATP and Mg^{2+} and, when initiated with CDP, yield dCDP as a product. ATP, CDP and dCDP each have distinctive NMR peaks making it possible to monitor the progress of a RNR reaction real-time. Figure 5 shows the extent of dCDP production and CDP consumption when the RNR reaction was quenched after 1 h. Addition of

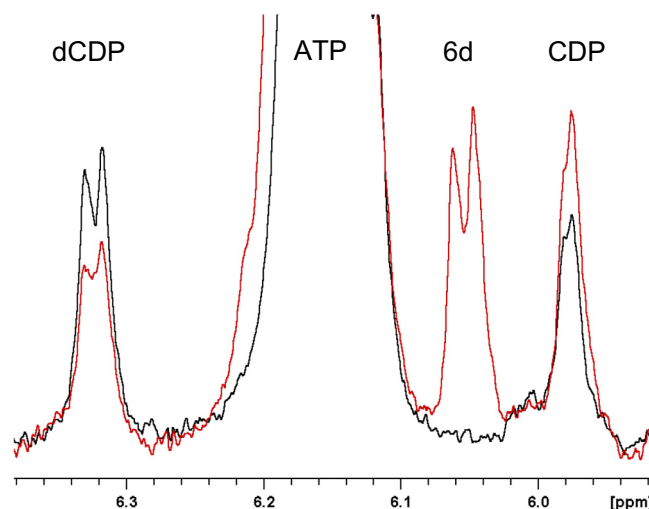


Figure 5. Inhibition of active RNR. Reaction products from active RNR are detected by ^1H NMR. 61 μM of dCDP is produced by RNR 1 h after the reaction was initiated with 100 μM CDP (black). Addition of 100 μM **6d** inhibits RNR resulting in a 32% reduction of dCDP production.

Table 2
Quantitation (AUC) of dNTP & NTP pools in the CEM cells

dNTPs & NTPs	Untreated	6d (1 μ M)
dCTP	0.11 \pm 0.01	0.03 \pm 0.01
dGTP	0.09 \pm 0.03	0.03 \pm 0.01
dATP	0.60 \pm 0.11	0.14 \pm 0.02
dTTP	0.25 \pm 0.09	0.11 \pm 0.03
CTP	2.68 \pm 0.09	1.48 \pm 0.14
GTP	4.00 \pm 0.13	1.25 \pm 0.04
ATP	38.89 \pm 2.50	17.83 \pm 0.86
UTP	10.05 \pm 0.56	3.59 \pm 0.31

Analyses performed in triplicate.

\pm Denotes standard deviation.

Units of measurement are AUC (area under the curve).

100 μ M **6d** yielded 32% inhibition of dCDP production and 32% reduction of CDP consumption when compared with control spectra.

The combination of binding and functional NMR data establishes that **6d** binds to the active site of RRM1, competes with the substrate and products for binding to the inactive enzyme and inhibits active RNR in vitro.

3.4. dNTP suppression studies

Studies have shown that GEM treatment suppresses dCTP, dGTP, and dATP pools.^{36–38} To confirm effects on dNTP levels, we compared **6d** with gemcitabine, using an HPLC-based assay.³⁹ In CEM control cells, dGTP was the smallest dNTP pool on the basis of AUC (area under the curve) (0.09 AUC \pm 0.03), compared with dCTP (0.11 AUC \pm 0.01), dATP (0.6 AUC \pm 0.11), dTTP (0.25 AUC \pm 0.09) (Table 2). Treatment with **6d** resulted in depletion of dATP, dCTP, dGTP (Table 2). Thus, treatment of cells with **6d** for 2 h leads to suppression of discrete dNTP pools (see Table 2).

4. Discussion

The ribonucleotide reductase (RNR) enzyme is a heteromer of RRM1 and RRM2 subunits where the active enzyme catalyzes de novo reduction of ribonucleotides to generate deoxyribonucleotides (dNTPs), which are required for DNA replication and DNA repair processes. Complexity in the generation of physiologically relevant, active RRM1/RRM2 heterodimers was perceived as limiting to the identification of selective RRM1 inhibitors by high-throughput screening of compound libraries and led us to seek alternative methods to identify lead series. We found that gemcitabine, as its diphosphate metabolite, represents one of the few described active site inhibitors of RRM1. However, due to the perceived requirement for phosphorylation of the 5'-OH of gemcitabine to initiate the production of active NDP and NTP metabolites, replacement of the 5'-OH has been left virtually unexplored. Towards the identification of selective RRM1 inhibitors, we hypothesized that gemcitabine diphosphate might serve as an effective template for the identification of such molecules. Thus, identification of 5'-substitution in replacement of the diphosphate with limited other structural changes may lead to effective competitors with the natural ligand. Likewise, the inability to form the triphosphate metabolite in situ would make these 5'-analogs devoid of competing incorporation into DNA.

Towards this end, we prepared a novel series of 5'-amino derivatives of gemcitabine that could catalyze binding to RRM1 using the synthetic methods described in Scheme 1. This series of 5'-amino gemcitabine analogs was demonstrated to be potent RRM1 inhibitors thru a combination of in-cell phenotypic screening, NMR studies, as well as functional readouts to confirm this finding.

In order to evaluate these derivatives for biological activity, we established the viability of using a previously established functional readout by monitoring gamma H2AX induction following treatment of replication inhibitor hydroxyurea and the CHK1 inhibitor, SCH 900776. Using this in-cell assay, we noted dose-dependent induction of γ -H2AX for this series of compounds (Fig. 1) and could rank order the derivatives based upon how robust the activity was observed. Based upon the response in this assay, **6d** was selected as a representative example for further characterization in order to establish that this series of compounds was behaving in a mechanistically similar way to gemcitabine diphosphate. Towards this end, a series of NMR experiments were conducted to establish ligand binding to RRM1. Small molecule line broadening was detected in the ¹H NMR spectra of **6d** (Fig. 2) in the presence of RRM1 and the resultant ligand signal reduction (27%) are consistent with protein binding at an approximate K_d of 200 μ M. Furthermore, saturation transfer difference NMR (STD-NMR) analysis revealed a new set of STD-NMR signals for **6d** which could be attributed to binding to RRM1. In addition, there was a decrease of the CDP STD-NMR signal due to competition by the ligand ($K_i \sim 150 \mu$ M) with CDP indicative of the binding of ligand to RRM1. The RRM1-bound conformation of **6d** was measured by transferred NOESY experiments. A single experiment was conducted with ligand and RRM1 which demonstrated ligand NOEs that were of the opposite sign of the free ligand NOE's which confirms RRM1 binding to both ATP and ligand. Finally, ¹H NMR measurements demonstrated 32% inhibition of dCDP production and 32% reduction of CDP consumption compared to control spectra giving a convenient readout of RNR activity. The combination of binding and functional NMR established that **6d** binds to the active site of RRM1, effectively competes with both substrate and product binding to inactive enzyme, and inhibits active RNR in vivo. Finally, **6d** was shown to reduce dNTP pools in U2OS cells consistent with observations made for gemcitabine using an HPLC method.

5. Conclusions

In summary, we have demonstrated that a series of novel 5'-amino gemcitabine analogs are potent RRM1 inhibitors through a combination of in-cell phenotypic screening, direct binding NMR studies, and in vivo dNTP reduction studies. These analogs offer great promise as novel therapeutics for cancer and additional work in this vein will be described in due course.

6. Experimentals

6.1. Biology experimentals

6.1.1. γ -H2AX assay

Briefly, analogs were titrated onto cells to induce the activation of CHK1. Control populations were left untreated. SCH 900776 was then added to cells over a two hour exposure window (in the presence of the analog). Following the 2 h co-exposure to SCH 900776, cells were fixed and permeabilized (70% ethanol) before staining with a FITC-conjugated anti- γ -H2AX monoclonal antibody (Millipore). Cells were counterstained with propidium iodide and subsequently analyzed using flow cytometry (Becton Dickinson LSR II) or the Discovery 1 immunofluorescence platform (Molecular Devices). Data are presented as the percentage of γ -H2AX positive cells, and thus reflect the overall penetrance of the γ -H2AX phenotype.

6.1.2. NMR spectroscopy

All data was collected at 27 $^{\circ}$ C on a Bruker Avance DRX 500 spectrometer using a 5 mm TXI cryoprobe. Binding and structural

studies were carried out on yeast-RRM1 protein in 50 mM Na_2HPO_4 D_2O buffer, pH 7.4 with 5 mM d-DTT and 5 mM MgCl_2 . Line broadening of **6d** was measured in ^1H -NMR spectra with and without protein. Competition STD NMR measurements were carried out using 0.9 μM RRM1 with 200 μM ATP, 200 μM CDP with and without 200 μM **6d**. Transferred NOESY data were collected on a sample of 9 μM RRM1, 200 μM ATP and 200 μM **6d** using a mix times ranging from 75 to 200 ms.

6.1.3. Functional RNR assay with NMR readout

Reactions were performed using human RNR proteins at 27 °C. The reaction buffer consisted of 50 mM d-Tris (D_2O), pH 7.6, 10 mM d-DDT, 70 μM $\text{Fe}(\text{NH}_4)(\text{SO}_4)_2$ and 6 mM MgCl_2 . Compound **6d** was incubated for 30 min with active RNR enzyme (0.8 μM RRM1, 5.6 μM RNR2) and 1 mM ATP. Reactions were initiated with the addition of 200 μM CDP and quenched by heating after 1 h. CDP consumption and dCDP production were measured by ^1H NMR with 25 μM TSP added as an internal standard. Percent inhibition with **6d** was compared to a reference spectrum where active RNR was incubated with d-DMSO. Reaction controls include dATP, didox and gemcitabine diphosphate.

6.1.4. Cell lines

Tumor cell lines were obtained from the American Type Culture Collection (ATCC) and cultured under the suggested growth conditions.

6.1.5. NTP/dNTP extraction

NTP/dNTP Extraction was performed as described previously.³⁹ The cell pellets were resuspended in ice-cold ultrapure water and deproteinized with equal volume of 6% TCA. Acid cell extracts (corresponding to 1×10^7 cells/ 80 μL) were vortexed for 20 s, ice bathed for 10 min, vortexed again for 20 s, and then centrifuged at 13,000 rpm for 10 min at 4 °C. The resulting supernatants were frozen on dry-ice and stored at -80 °C prior to analysis. Before HPLC analysis, samples were thawed and aliquots of 60 μL were neutralized with 0.5 μL of 0.67% NH_4OH . 50 μL of this solution was injected onto the HPLC column. All experiments were done in triplicate.

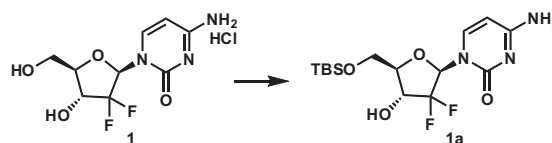
6.1.6. Instrument and chromatographic conditions and measurement of NTP/dNTP levels

The chromatographic system consisted of an HPLC Ettan LC (GE Healthcare) with a Halo column from MacMod Analytical 2.7 μm (4.6×150 mm). The column was kept at room temperature. The mobile phase was delivered using the following linear gradient elution program (rinsing and reequilibration steps included): (% Buffer A/% Buffer B), flow rate of 1 mL/min (100:0) to (30:70) in 20 min → flow rate of 0.9 mL/min (30:70) to (0:100) in 12 min → flow rate of 0.9 mL/min hold at (0:100) for 10 min → flow rate of 0.5 mL/min (0:100) to (50:50) in 5 min → flow rate of 1 mL/min (100:0) for 10 column volumes.

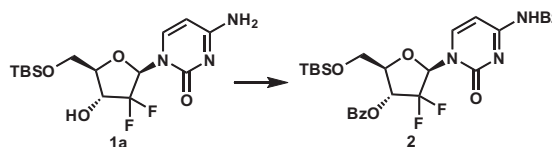
Buffer A contained 10 mM tetrabutylammonium hydroxide, 10 mM KH_2PO_4 and 0.25% MeOH, and adjusted to pH 7.0 with 1 M HCl. Buffer B contained 5.6 mM tetrabutylammonium hydroxide, 50 mM KH_2PO_4 and 30% MeOH, and adjusted to pH 7.0 with 1 M NaOH. Both Buffer A and B were made fresh for experiment and passed through 0.22 μm filters to avoid microbial contamination. Both solvents were degassed. The injection volume was 50 μL . Detection was UV absorption at 260 nm. Chromatograms are analyzed for peak integration on Unicorn version 5.2 (GE Healthcare) to calculate the area under the curve to quantitate the levels of dNTPs (dCTP, dGTP, dATP, dTTP) and for the NTPs (CTP, GTP, ATP, UTP) in U2OS cells.

6.2. Chemistry experimentals

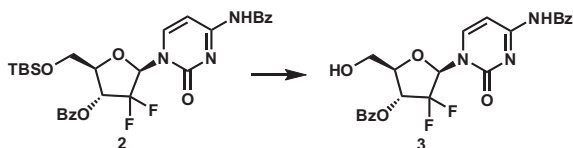
Mass spectra were recorded using either an EXTREL 401 (CI), JEOL or MAT-90 (FAB), VG, ZAB-SE (SIMS) or Finnigan MAT-CH-% (EI) spectrometer. NMR structure determinations of the compounds were made using chemical shifts, coupling constants, coupling information from COSY spectra, and 1D NOE experiments. ^1H NMR and ^{13}C NMR spectra were obtained on Varian XL 400 (400 MHz, ^1H ; 100 MHz, ^{13}C) and are reported as ppm down field from Me_4Si with number of protons, multiplicities, and coupling constants in Hertz indicated parenthetically. For ^{13}C NMR, a Nalorac Quad nuclei probe was used. Compound purity was checked by TLC and LC/MS analysis using an Applied Biosystems API-100 mass spectrometer and Shimadzu SCL-10A LC column: Altech platinum C18, 3 micron, 33 mm \times 7 mm ID; gradient flow: 0 min–10% CH_3CN , 5 min–95% CH_3CN , 7 min–95% CH_3CN , 7.5 min–10% CH_3CN , 9 min stop. Chromatography was performed with Selecto Scientific flash silica gel, 32–63 μm .



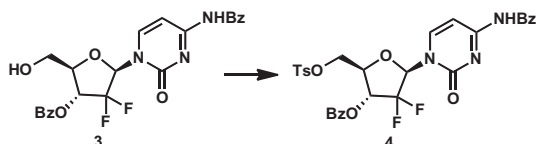
Compound **1a**: A solution of gemcitabine-hydrochloride (10.9 g, 36.6 mmol) in DMF (80 mL) at 25 °C was treated successively with imidazole (7.4 g, 109 mmol) and *tert*-butyldimethylsilyl chloride (6.0 g, 40 mmol). The solution was stirred at 25 °C for 15 h whereupon the reaction mixture was concentrated under reduced pressure. The resultant material was purified by silica gel chromatography using a gradient of 5–20% MeOH in CH_2Cl_2 to provide **1a** (13.4 g, 98%) as a clear oil. ^1H NMR ($\text{DMSO}-d_6$) δ 7.64 (1H, d, $J = 7.7$ Hz), 7.41 (2H, br s), 6.14 (1H, dd, $J = 7.9, 7.6$ Hz), 5.76 (1H, d, $J = 7.7$ Hz), 4.12 (1H, m), 3.94 (1H, br d, $J = 12.4$ Hz), 3.86 (1H, m), 3.80 (1H, dd, $J = 12.4, 3.0$ Hz), 0.89 (9H, s), 0.086 (6H, s). Mass calculated for formula $\text{C}_{15}\text{H}_{25}\text{F}_2\text{N}_3\text{O}_4\text{Si}$ 377.2, observed LCMS m/z 378.3 (M+H).



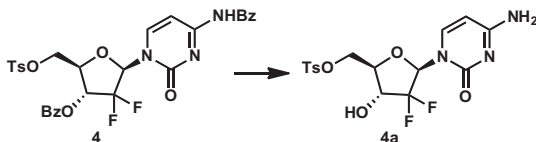
Compound **2**: To a solution of silyl ether **1a** (5.88 g, 15.6 mmol) in pyridine (78 mL) at 25 °C was added 4-dimethylaminopyridine (3.81 g, 31.2 mmol) portionwise followed by dropwise addition of benzoyl chloride (7.2 mL, 62.2 mmol). The resultant solution was stirred at 25 °C for 15 h whereupon the reaction was quenched with water. The crude reaction mixture was extracted with EtOAc and the organic layers were combined. The organic layer was washed with 5% aqueous NaHCO_3 solution, brine solution, dried over Na_2SO_4 , and concentrated in vacuo. The resultant residue was purified by silica gel chromatography with a gradient of 10–100% EtOAc/hexane provided compound **2** (7.8 g, 85%). ^1H NMR (CDCl_3) δ 8.74 (1H, br s), 8.17 (1H, br d, $J = 7.0$ Hz), 8.09 (2H, dd, $J = 8.3, 1.5$ Hz), 7.91 (2H, br d, $J = 7.1$ Hz), 7.63 (2H, m), 7.54–7.48 (5H, m), 6.58 (1H, t, $J = 8.0$ Hz), 5.74 (1H, m), 4.34 (1H, m), 4.08 (1H, dd, $J = 12.0, 2.3$ Hz), 3.95 (1H, dd, $J = 12.0, 2.5$ Hz), 0.96 (9H, s), 0.16 (6H, s). Mass calculated for formula $\text{C}_{29}\text{H}_{33}\text{F}_2\text{N}_3\text{O}_6\text{Si}$ 585.2, observed LCMS m/z 586.2 (M+H).



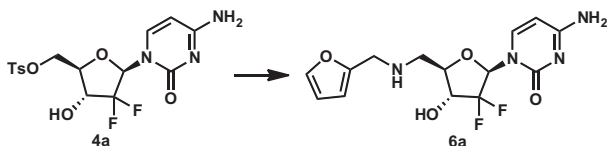
Compound 3: To a solution of the silyl ether **2** (7.9 g, 13.5 mmol) in THF (270 mL) at 0 °C was added a 1.0 M solution of tetrabutylammonium fluoride in THF (14.9 mL, 14.9 mmol). The solution was stirred at 0 °C for 3.5 h and then quenched with AcOH (1.16 mL, 20.3 mmol) and water (600 mL). EtOAc (200 mL) was added and the organic layer was collected. The aqueous layer was extracted with EtOAc (2 × 50 mL). The organic layers were combined, washed with brine, dried over Na₂SO₄ and concentrated in vacuo. Trituration of the residue with CH₂Cl₂ followed by filtration provided alcohol **3** (5.4 g, 85%) as a white solid. ¹H NMR (DMSO-*d*₆) δ 11.50 (1H, br s), 8.36 (1H, br d, *J* = 7.3 Hz), 8.12 (2H, dd, *J* = 8.2, 1.2 Hz), 8.06 (2H, dd, *J* = 8.2, 1.2 Hz), 7.80 (1H, m), 7.69 (1H, m), 7.65 (2H, m), 7.57 (2H, m), 7.50 (1H, br d, *J* = 6.8 Hz), 6.49 (1H, t, *J* = 8.7 Hz), 5.68 (1H, m), 5.43 (1H, br s), 4.55 (1H, m), 3.91 (1H, br d, *J* = 12.4 Hz), 3.81 (1H, br d, *J* = 12.4 Hz). Mass calculated for formula C₂₃H₁₉F₂N₃O₆ 471.1, observed LCMS *m/z* 472.0 (M+H).



Compound 4: A solution of alcohol **3** (2.65 g, 5.62 mmol) in pyridine (56 mL) at 0 °C was treated successively with *p*-toluenesulfonyl chloride (4.27 g, 31.6 equiv) and triethylamine (1.55 mL, 15.8 equiv). The solution was stirred at 0 °C for 3 h and the ice bath was removed and stirring was continued at 25 °C for 15 h. The solution was concentrated and the residue was purified using silica gel chromatography with a gradient of 0–25% acetone in CH₂Cl₂ to afford tosylate **4** as a white solid (3.06 g, 87%). Mass calculated for formula C₃₀H₂₅F₂N₃O₈S 625.6, observed LCMS *m/z* 626.1 (M+H).

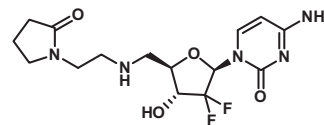


Compound 4a: A solution of tosylate **4** (2.06 g, 3.29 mmol) in 7 N NH₃ in MeOH solution (100 mL) was stirred at 25 °C for 2 h. The solution was concentrated and the residue was purified using silica gel chromatography with a gradient 10–30% MeOH in CH₂Cl₂ to afford compound **4a** as white solid (0.80 g, 58%) after concentration. Mass calculated for formula C₁₆H₁₇F₂N₃O₆S 417.1, observed LCMS *m/z* 418.0 (M+H). This material was used crude in the next transformation without purification.

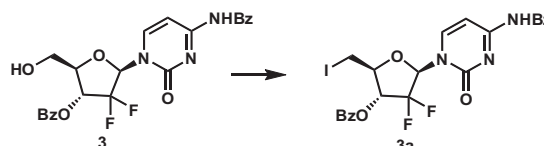


Compound 6a: A solution of tosylate **4a** (80 mg, 0.19 mmol) and 2-furylmethylamine (0.085 mL, 0.99 mmol) in DMF (0.2 mL), in a sealed tube, was heated at 100 °C for 3 h. The solution was cooled to room temperature and concentrated under reduced pressure. The residue was purified using silica gel chromatography with a gradient of 0–40% MeOH in CH₂Cl₂ whereupon a white solid (21 mg,

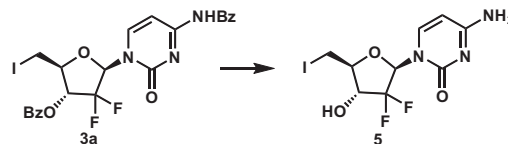
32%) was obtained. ¹H NMR (CD₃OD) δ 7.67 (d, *J* = 8.0 Hz, 1H), 7.44 (d, *J* = 2.2 Hz, 1H), 6.25–6.36 (m, 1H), 6.27 (d, *J* = 3.6 Hz, 1H), 6.18 (t, *J* = 8.0 Hz, 1H), 5.90 (d, *J* = 7.3 Hz, 1H), 4.07–4.14 (m, 1H), 3.91–3.96 (m, 1H), 3.83 (s, 2H), 3.03 (dd, *J* = 2.9 Hz, *J* = 13.9 Hz, 1H), 2.94 (dd, *J* = 6.6 Hz, *J* = 13.2 Hz, 1H). Mass calculated for formula C₁₄H₁₆F₂N₄O₄ 342.1, observed LCMS *m/z* 343.0 (M+H).



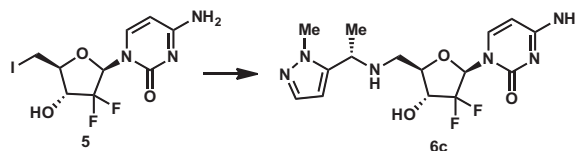
Compound 6b: Using the procedure outlined for the preparation of Compound **6a**, treatment of tosylate **4** (67 mg, 0.19 mmol) with 1-(2-aminoethyl)pyrrolidin-2-one (0.20 g, 1.6 mmol) afforded **6b** (32 mg, 53%) as a white solid. ¹H NMR (400 MHz, CD₃OD) δ 7.67 (d, *J* = 7.5 Hz, 1H), 6.20 (t, *J* = 8.4 Hz, 1H), 5.94 (d, *J* = 7.5 Hz, 1H), 4.08–4.14 (m, 1H), 3.91–3.95 (m, 1H), 3.49 (t, *J* = 7.0 Hz, 2H), 3.34–3.44 (m, 2H), 3.07 (dd, *J* = 3.3, 13.4 Hz, 1H), 2.95 (dd, *J* = 6.6, 13.4 Hz, 1H), 2.79–2.88 (m, 2H), 2.34–2.40 (m, 2H), 2.01–2.08 (m, 2H). mass calculated for C₁₅H₂₁F₂N₅O₄ 373.2, observed LCMS *m/z* 374.2 (M+H).



Compound 3a: Into a round-bottom flask was added compound **3** (5.3 g, 11.24 mmol), methyltriphenoxyphosphonium iodide (12.0 g, 26.54 mmol) and DMF (80 mL). The reaction mixture was stirred at 60 °C overnight and quenched with methanol. The crude mixture was concentrated, diluted with dichloromethane (200 mL), and washed with 5% sodium thiosulfate solution (2 × 100 mL) and brine (3 × 100 mL), dried over Na₂SO₄, filtered and concentrated. The residue was purified by column chromatography (SiO₂, 12–16% ethyl acetate/DCM) to afford **3a** (5.47 g; 84%) as a white solid. Mass calculated for formula C₂₃H₁₈F₂IN₃O₅ 581.03, observed LCMS *m/z* 582.1 (M+H).

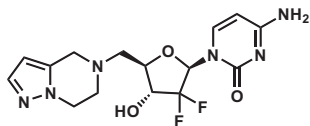


Compound 5: To a pressure bottle was added compound **3a** (5.40 g, 9.29 mmol) followed by 7 M NH₃ in methanol (210 mL, 1470 mmol). The heterogeneous mixture became clear 30 min later, and was kept stirring at rt for 2 h. The solution was concentrated and purified by column chromatography (SiO₂, 10–15% methanol/DCM) to afford **5** (3.19 g; 92%) as a white solid. Mass calculated for formula C₉H₁₀F₂IN₃O₃ 373.0, observed LCMS *m/z* 374.0 (M+H).



Compound 6c: Compound **5** (3.04 g, 8.15 mmol) in DMF (3 mL) was treated with (*S*)-1-(1-methyl-1H-pyrazol-5-yl)ethanamine (3.43 g, 27.4 mmol) in a 20 mL vial, and was heated to 90 °C for 3.5 h. The mixture was concentrated and purified by column chromatography (SiO₂, 15% methanol/DCM), followed by lyophilization to afford **6c** (1.6 g, 53%) as a white solid. ¹H NMR (400 MHz, CD₃OD) δ 7.58

(1H, d, $J = 7.4$ Hz), 7.38 (1H, d, $J = 2.0$ Hz), 6.25 (1H, d, $J = 2.0$ Hz), 6.18 (1H, t, $J = 8.6$ Hz), 5.86 (1H, d, $J = 7.4$ Hz), 4.13 (1H, q, $J = 6.8$ Hz), 4.06 (1H, m), 3.91 (1H, m), 3.82 (3H, s), 2.95 (1H, dd, $J = 13.2, 3.2$ Hz), 2.86 (1H, dd, $J = 13.2, 6.4$ Hz), 1.40 (3H, d, $J = 6.8$ Hz). Mass calculated for formula $C_{15}H_{20}F_2N_6O_3$ 370.2, observed LCMS m/z 371.2 (M+H).



Compound 6d: Using the procedure outlined for the preparation of Compound **6c**, treatment of compound **5** (98 mg, 0.26 mmol) with 4,5,6,7-tetrahydropyrazolo[1,5-a]pyridazine (0.10 g, 83 mmol) afforded **6d** (46 mg, 48%) as a white solid. 1H NMR (400 MHz, CD_3OD) δ 8.14 (d, $J = 8.2$ Hz, 1H), 7.62 (d, $J = 2.1$ Hz, 1H), 6.34 (d, $J = 2.1$ Hz, 1H), 6.27 (t, $J = 7.9$ Hz, 1H), 6.22 (d, $J = 8.2$ Hz, 1H), 4.80 (bm, 2H), 4.58–4.47 (m, 3H), 4.42–4.36 (m, 1H), 4.05 (t, $J = 5.4$ Hz, 2H), 4.01–3.88 (m, 2H). Mass calculated for formula $C_{15}H_{18}F_2N_6O_3$ 368.14, observed LCMS m/z 369.2 (M+H).

References and notes

- Nordlund, P.; Reichard, P. *Annu. Rev. Biochem.* **2006**, *75*, 681.
- Cory, J. G.; Sato, A. *Mol. Cell. Biochem.* **1983**, *53–54*, 257.
- Thelander, L.; Reichard, P. *Annu. Rev. Biochem.* **1979**, *48*, 133.
- Chabes, A.; Georgieva, B.; Domkin, V.; Zhao, X.; Rothstein, R.; Thelander, L. *Cell* **2003**, *112*, 391.
- Reichard, P. *Annu. Rev. Biochem.* **1988**, *57*, 349.
- Thelander, M.; Gräslund, A.; Thelander, L. *J. Biol. Chem.* **1985**, *260*, 2737.
- Tanaka, H.; Arakawa, H.; Yamaguchi, T.; Shiraiishi, K.; Fukuda, S. *A. Nature* **2000**, *404*, 42.
- Guittet, O.; Håkansson, P.; Voevodskaya, N.; Fridt, S.; Gräslund, A.; Arakawa, H.; Nakamura, Y.; Thelander, L. *J. Biol. Chem.* **2001**, *274*, 40637.
- Szekeres, T.; Fritzer-Szekeres, M.; Elford, H. L. *Crit. Rev. Clin. Lab. Sci.* **1997**, *34*, 503.
- Nocentini, G. *Crit. Rev. Oncol. Hematol.* **1996**, *22*, 89.
- Lien, E. J. *Prog. Drug Res.* **1987**, *31*, 101.
- Shao, J.; Zhou, B.; Chu, B.; Yen, Y. *Curr. Cancer Drug Targets* **2006**, *6*, 409.
- Gandhi, V.; Plunkett, W. *Biochem. Pharmacol.* **1989**, *38*, 3551.
- Xie, K. C.; Plunkett, W. *Cancer Res.* **1996**, *56*, 3030.
- Sampath, D.; Rao, V. A.; Plunkett, W. *Oncogene* **2003**, *22*, 9063.
- Ewald, B.; Sampath, D.; Plunkett, W. *Mol. Cancer Ther.* **2007**, *6*, 1239.
- Lopes, M.; Cotta-Ramusino, C.; Pelliccioli, A.; Liberi, G.; Plevani, P.; Muzi-Falconi, M.; Newion, C. S.; Folani, M. *Nature* **2001**, *412*, 557.
- (a) Burris, H. A., III; Moore, M. J.; Andersen, J.; Green, M. R.; Rothenberg, M. L.; Modiano, M. R.; Cripps, M. C.; Portenoy, R. K.; Storniolo, A. M.; Tarassoff, P.; Nelson, R.; Dorr, F. A.; Stephens, C. D.; Von Hoff, D. D. *J. Clin. Oncol.* **1997**, *15*, 2403; (b) Manegold, C. *Expert Rev. Anticancer Ther.* **2004**, *4*, 345; (c) Heinemann, V. *Expert Rev. Anticancer Ther.* **2005**, *5*, 429.
- Heinemann, V.; Hertel, L. W.; Grindey, G. B.; Plunkett, W. *Cancer Res.* **1988**, *48*, 4024.
- (a) van der Donk, W. A.; Yu, G.; Pérez, L.; Sanchez, R. J.; Stubbe, J.; Samano, V.; Robins, M. J. *Biochemistry* **1998**, *37*, 6419; (b) Artin, E.; Wang, J.; Lohman, G. J. S.; Yokoyama, K.; Yu, G.; Griffin, R. G.; Bar, G.; Stubbe, J. *Biochemistry* **2009**, *48*, 11622.
- Huang, P.; Chubb, S.; Hertel, L. W.; Grindey, G. B.; Plunkett, W. *Cancer Res.* **1991**, *51*, 6110.
- Hertel, L. W.; Kroin, J. S.; Misner, J. W.; Tustin, J. M. *J. Org. Chem.* **1988**, *53*, 2406.
- (a) Hertel, L. W.; Grossman, C. S.; Kroin, J. S.; Mineishib, S.; Chubb, S.; Nowak, B.; Plunkett, W. *Nucleosides Nucleotides* **1989**, *8*, 951; (b) Fahrig, R.; Lohmann, D.; Rolfs, A.; Dieks, H.; Teubner, J.; Heinrich, J.-C. WO 2008017515, 2008; *Chem. Abstr.* **2008**, *148*, 239457.
- Smith, D. B.; Kalayanov, G.; Sund, C.; Winqvist, A.; Maltseva, T.; Leveque, V. J.-P.; Rajyaguru, S.; Le Pogran, S.; Najera, I.; Benkestock, K.; Zhou, Z.; Kaiser, A. C.; Maag, H.; Cammack, N.; Martin, J. A.; Swallow, S.; Johansson, N. G.; Klumpp, K.; Smith, M. J. *Med. Chem.* **2009**, *52*, 2971.
- Qiu, Y.-L.; Wang, C.; Peng, X.; Ying, L.; Or, Y. S. WO 2010030858, 2010; *Chem. Abstr.* **2010**, *152*, 335423.
- Hertel, L. W.; Grossman, C. S.; Kroin, J. S. EP 329348, 1989; *Chem. Abstr.* **1989**, *112*, 56592.
- (a) Qiu, X.-L.; Xu, X.-H.; Qing, F.-L. *Tetrahedron* **2010**, *66*, 789; (b) Devos, R.; Dymock, B. W.; Hobbs, C. J.; Jiang, W.-R.; Martin, J. A.; Merrett, J. H.; Najera, I.; Shamma, N.; Tsukuda, T. WO 2002018404, 2002; *Chem. Abstr.* **2002**, *136*, 217007.
- Guzi, T. J.; Parry, D. A.; Labroli, M. A.; Dwyer, M. P.; Paruch, K.; Rosner, K. E.; Shen, R.; Popovici-Muller, J. WO 2009061781, 2009; *Chem. Abstr.* **2009**, *150*, 515402.
- Eriksson, M.; Uuhlin, U.; Ramaswamy, S.; Ekberg, M.; Regnström, K. *Structure* **1997**, *5*, 1077.
- Labroli, M. A.; Dwyer, M. P.; Shen, R.; Popovici-Muller, J.; Pu, Q.; Richard, J.; Rosner, K.; Paruch, K.; Guzi, T. J. *Tetrahedron Lett.* **2014**, *55*, 598.
- Guzi, T. J.; Paruch, K.; Dwyer, M. D.; Labroli, M. A.; Shanahan, F.; Davis, N.; Taricani, L.; Wiswell, D.; Seghezzi, W.; Penafior, E.; Bhagwat, B.; Wang, W.; Gu, D.; Hsieh, Y.; Lee, S.; Liu, M.; Parry, D. *Mol. Cancer Ther.* **2011**, *10*, 591.
- Shortridge, M. D.; Hage, D. S.; Harbison, G. S.; Powers, R. J. *Comb. Chem.* **2008**, *10*, 948.
- Mayer, M.; Meyer, B. A. *Angew. Chem., Int. Ed.* **1998**, *38*, 1784.
- McCoy, M. A.; Senior, M. M.; Wyss, D. F. *J. Am. Chem. Soc.* **2005**, *127*, 7978.
- Fisher, A.; Laub, P. B.; Cooperman, B. S. *Nat. Struct. Biol.* **1995**, *11*, 951.
- Cooper, T.; Ayres, M.; Nowak, B.; Gandhi, V. *Cancer Chemother. Pharmacol.* **2005**, *55*, 361.
- Gandhi, V.; Mineishi, S.; Huang, P.; Yang, Y.; Chubb, S.; Chapman, A. J.; Nowak, B. J.; Hertel, L. W.; Plunkett, W. *Semin. Oncol.* **1995**, *22*, 61.
- Heinemann, V.; Schulz, L.; Issels, R. D.; Plunkett, W. *Semin. Oncol.* **1995**, *22*, 11.
- Decosterd, L. A.; Cottin, E.; Chen, X.; Lejeune, F.; Mirimanoff, R. O.; Biollaz, J.; Coucke, P. A. *Anal. Biochem.* **1999**, *270*, 59.